

Satiated Relative Permeability of Variable- Aperture Fractures

R. L. Detwiler, R. J. Glass, H. Rajaram, M. J. Nicholl

This article was submitted to
International Groundwater Symposium, Berkeley, CA, March 25-28,
2002

December 11, 2001

U.S. Department of Energy

Lawrence
Livermore
National
Laboratory

DISCLAIMER

This document was prepared as an account of work sponsored by an agency of the United States Government. Neither the United States Government nor the University of California nor any of their employees, makes any warranty, express or implied, or assumes any legal liability or responsibility for the accuracy, completeness, or usefulness of any information, apparatus, product, or process disclosed, or represents that its use would not infringe privately owned rights. Reference herein to any specific commercial product, process, or service by trade name, trademark, manufacturer, or otherwise, does not necessarily constitute or imply its endorsement, recommendation, or favoring by the United States Government or the University of California. The views and opinions of authors expressed herein do not necessarily state or reflect those of the United States Government or the University of California, and shall not be used for advertising or product endorsement purposes.

This is a preprint of a paper intended for publication in a journal or proceedings. Since changes may be made before publication, this preprint is made available with the understanding that it will not be cited or reproduced without the permission of the author.

This work was performed under the auspices of the United States Department of Energy by the University of California, Lawrence Livermore National Laboratory under contract No. W-7405-Eng-48.

This report has been reproduced directly from the best available copy.

Available electronically at <http://www.doc.gov/bridge>

Available for a processing fee to U.S. Department of Energy
And its contractors in paper from
U.S. Department of Energy
Office of Scientific and Technical Information
P.O. Box 62
Oak Ridge, TN 37831-0062
Telephone: (865) 576-8401
Facsimile: (865) 576-5728
E-mail: reports@adonis.osti.gov

Available for the sale to the public from
U.S. Department of Commerce
National Technical Information Service
5285 Port Royal Road
Springfield, VA 22161
Telephone: (800) 553-6847
Facsimile: (703) 605-6900
E-mail: orders@ntis.fedworld.gov
Online ordering: <http://www.ntis.gov/ordering.htm>

OR

Lawrence Livermore National Laboratory
Technical Information Department's Digital Library
<http://www.llnl.gov/tid/Library.html>

Satiated Relative Permeability of Variable-Aperture Fractures

Russell L. Detwiler^{1,4}, Robert J. Glass², Harihar Rajaram¹ and Michael J. Nicholl³

1 Department of Civil, Environmental and Architectural Engineering, University of Colorado, Boulder, Colorado.

2 Flow Visualization and Processes Laboratory, Sandia National Laboratories, Albuquerque, New Mexico.

3 Department of Materials, Metallurgical, Mining, and Geological Engineering, University of Idaho, Moscow, Idaho.

4 Now at: Division of Geophysics and Global Security, Lawrence Livermore National Laboratory, Livermore, California.

Abstract

The relative permeability of a variable-aperture fracture under satiated conditions (wetting phase spans the fracture, non-wetting phase is completely entrapped) is controlled by the distribution of the entrapped phase within the fracture plane. We use simulations to investigate the combined influence of capillary forces and aperture variability on satiated relative permeability and demonstrate the effectiveness of a dimensionless perturbation curvature number (C') for predicting entrapped-phase structure. C' combines the relative influence of in-plane and out-of-plane interface curvature and the aperture coefficient of variation ($\sigma_a / \langle a \rangle$) on local capillary forces. Results suggest that C' provides a single parameter that can be used to estimate satiated relative permeability.

1.0 Introduction

In a statistically homogeneous, horizontal, initially dry, variable-aperture fracture that is much larger than the correlation scale of aperture variability, slow invasion of a wetting fluid results in a *satiated* condition: the wetting fluid completely spans the fracture and the non-wetting fluid is fully entrapped. The satiated relative permeability (k_{rw}) relates the transmissivity of the wetting fluid in the satiated fracture to the fully saturated transmissivity of the fracture. *Nicholl et al.* [2000] compared experimental measurements of flow through a satiated fracture to flow simulations (based on the depth-averaged Reynolds equation) in measured aperture and phase-distribution fields. This comparison demonstrated that simulated estimates of satiated relative permeability closely matched the corresponding experimental measurements. They also presented a conceptual model for k_{rw} that suggested that increased tortuosity and decreased wetting phase saturation induced by the entrapped phase are the primary contributions to reduction in k_{rw} . *Glass et al.* [1998, 2000] used a modified invasion percolation (MIP) algorithm to investigate the role of interfacial curvature on entrapped-phase structure; they demonstrated good agreement between experimentally observed and simulated phase structures.

In this paper, we use MIP simulations to systematically investigate the combined influence of capillary forces and aperture variability on entrapped-phase structure. Subsequent simulations of flow of the wetting phase provide measures of satiated relative permeability, which we compare to predictions from the conceptual model presented by *Nicholl et al.* [2000].

2.0 Mathematical development

2.1 Phase invasion

Under quasi-static flow conditions, capillary forces will control phase structure in a horizontal fracture; in general, the non-wetting phase will be found in large apertures and the wetting phase in small ones. *Glass et al.* [1998, 2000] used the Laplace-Young equation, which relates surface tension (ϕ) and interfacial curvature, as quantified by the two principle radii of curvature, r_1 and r_2 , to the pressure jump across the curved interface (P_c):

$$P_c = \phi \left(\frac{1}{r_1} + \frac{1}{r_2} \right) \quad (1)$$

to derive the MIP algorithm for simulating invasion of immiscible fluids in variable-aperture fractures. In equation (1), r_1 is measured normal to the plane of the fracture and r_2 is measured in the fracture plane (**Figure 1**). *Glass et al.* (1998, 2000) defined $r_1 = \frac{-a}{2 \cos(\alpha + \beta)}$ and

$r_2 = \langle r_2 \rangle \tan\left(\frac{\gamma}{2}\right)$, where a is the local aperture, α is the fluid/fluid/solid contact angle, β is the convergence/divergence angle of the fracture surfaces, $\langle r_2 \rangle$, the mean in-plane radius of curvature, is estimated as $\lambda/2$, and γ is a weighted measure of the local included angle of the interface. Substituting these expressions for r_1 and r_2 into (1) results in:

$$P_c = \phi \left(\frac{-2 \cos(\alpha + \beta)}{a} + \frac{2}{\lambda} \cot\left(\frac{\gamma}{2}\right) \right) \quad (2)$$

To facilitate design of parametric investigations of the role of phase structure on flow, transport, and interphase mass transfer, we rewrite (2) in terms of mean and perturbation equations, which yields a mean P_c along the invasion front of

$$\bar{P}_c = \phi \left[\frac{1}{\langle a \rangle} \right] \quad (3)$$

and perturbations of:

$$P_c' = \phi \left[\frac{-a'}{\langle a \rangle^2} + \frac{2}{\lambda} \cot\left(\frac{\gamma}{2}\right) \right] \quad (4)$$

where $\langle \rangle$ and $'$ represent the spatial average and perturbation, respectively. Equation (3) simply defines the mean P_c as a constant along the interface between the invading and defending fluids. Thus, it is the perturbations in P_c (P_c') that control the geometry of the resulting entrapped phase and the resulting saturated relative permeability. Equation (4), which results from a first-order Taylor series expansion of (2), inherently assumes small perturbations in a . Rewriting (4) as a dimensionless perturbation equation yields:

$$P_c'^* = -a'^* \text{sign}(\cos \alpha) + C' \frac{1}{r_2^*} \quad (5)$$

with:

$$P_c^* = \frac{\langle a \rangle^2}{2\sigma_a \phi |\cos \alpha|} P_c \quad a'^* = \frac{a'}{\sigma_a} \quad r_2^* = \tan\left(\frac{\gamma}{2}\right) \quad C' = \frac{\langle a \rangle^2}{\lambda \sigma_a |\cos \alpha|}$$

where $\langle a \rangle$ is the mean aperture and C' is the dimensionless perturbation curvature number, which is equal to $C/(\sigma_a/\langle a \rangle)$, where C is the curvature number presented by *Glass et al.* [1998, 2000]. Equation (5) suggests that the entrapped phase structures resulting from invasion of an immiscible fluid into a fracture will be a function of C' . Thus, for a given invasion process with any values of $\langle a \rangle$, σ_a , λ , and α that yield the same value of C' , the resulting entrapped phase structure should be identical. We evaluate this hypothesis through a series of numerical simulations in Section 3.

2.2 Fluid flow

Flow of the saturated wetting phase can be simulated using the Reynolds equation, a depth-averaged approximation to the three-dimensional Stokes equations, which is given by:

$$\nabla \cdot (T \nabla h) = 0 \quad (6)$$

where $T = a^3 g / 12 \nu$, h is the local pressure head, g is the gravitational constant, and ν is the kinematic viscosity and no-flux boundary conditions are specified at the interfaces between the flowing and entrapped phases. The ratio of the simulated flow-rate in the saturated fracture to that in the saturated fracture provides an estimate of the saturated relative permeability (k_{rw}) of a fracture occupied by a specific phase distribution. *Nicholl et al.* [2000] expanded on a theoretical expression for flow through a fracture with multiple contact areas [*Zimmerman and Bodvarsson*, 1996] resulting in a conceptual model of k_{rw} :

$$k_{rw} = \tau s_f \underbrace{\left[\frac{\langle a_f \rangle^2}{\langle a \rangle^2} \right]}_A \underbrace{\left[\left(1 + \frac{9\sigma_a^2}{\langle b \rangle^2} \right)^{1/2} \left(1 + \frac{9\sigma_{a_f}^2}{\langle b_f \rangle^2} \right)^{-1/2} \right]}_B \quad (7)$$

where τ is a tortuosity factor that quantifies the lengthening of flow paths through the fracture due to the entrapped phase, s_f is the saturation of the flowing fluid, part A quantifies the change in effective mean aperture available to the flowing phase, and part B quantifies the influence of changes in aperture variability due to the entrapped phase. *Nicholl et al.* [2000] found that the relative importance of the individual terms in (7) followed the order in which they are included in (7) – i.e. τ has the strongest influence on k_{rw} and part B has the weakest influence. We evaluate the ability of (7) to predict k_{rw} over a wide range of aperture-field statistics and entrapped-phase distributions.

3.0 Computational experiments

To evaluate the influence of C' on entrapped-phase distribution and the resulting relative permeability, we simulated invasion and subsequent flow of the saturated wetting phase in four synthetic aperture fields, each with a different value of $\sigma_a/\langle a \rangle$. To evaluate the ability of C' to predict the entrapped-phase structure, we simulated wetting-phase invasions into each aperture field over a range of C' . Subsequent flow simulations in each of the saturated aperture fields, allowed an evaluation of the ability of (7) to predict k_{rw} in a wide range of entrapped-phase distributions in aperture fields exhibiting a range of $\sigma_a/\langle a \rangle$.

3.1 Aperture fields

Brown [1995] proposed a simple model to describe two-dimensional fracture aperture fields that was based on a number of profilometry measurements of fracture surfaces. These measurements demonstrated that the power spectra of the fracture surface profiles obeyed a power law spectrum and demonstrated that aperture fields resulting from combining two of these surfaces would also have power spectra obeying power laws. However, due to the cross-correlation of the two fracture surfaces, the fracture aperture fields should exhibit a mismatch length-scale, or a length-scale above which the fracture surfaces are perfectly correlated and hence the aperture field is completely uncorrelated. We generated a 1024x2048, gaussian, random field with a mean of 0, and variance of 1 and a power spectrum of the form:

$$G(k_x, k_y) \propto \frac{1}{(1 + l^2 k_x^2 + l^2 k_y^2)^n} \quad (8)$$

where k_x and k_y are the wave numbers corresponding to the x and y -dimensions, n is an exponent in the range $1.0 < n < 1.5$ [*Brown*, 1995], and l is a cutoff length-scale. This functional form of G yields a smooth transition from the power law behavior ($k > 1/l$) to the cutoff value ($k < 1/l$) that results in random fields with well-behaved semivariograms (i.e. no oscillations as occur with an abrupt cutoff). The random field had a correlation length, λ , defined as the separation distance at which the semivariogram reached a value of $\sigma^2(1-1/e)$, of 5 grid-blocks, and $n=1.3$. We scaled this field to obtain 4 fields with $\sigma_a / \langle a \rangle = 0.0625, 0.125, 0.25, \text{ and } 0.5$. For the invasion and flow simulations described in the following section, $\langle a \rangle = 0.02$ cm and $\lambda = 0.075$ cm.

3.2 Invasion simulations

In each of the four aperture fields, we simulated invasion of a wetting phase into the initially non-wetting-phase-filled fracture for C' ranging from 0 to 8.58. $C' = 0$ corresponds to a standard invasion percolation model (i.e. P_c depends only on local aperture because r_2 is assumed infinite), so the distribution of the entrapped phase should be identical regardless of $\sigma_a / \langle a \rangle$ and for C' of 8.58 and larger, non-wetting phase fluid did not become entrapped within any of the aperture fields. During invasion, the wetting phase entered the fracture through one edge and the non-wetting phase was permitted to leave the fracture through each of the other three edges. **Figure 2** shows measurements of the areal portion of the fracture occupied by the flowing phase plotted against C' for each value of $\sigma_a / \langle a \rangle$. For the range $0 < C' < 0.5$, the entrapped area is insensitive to $\sigma_a / \langle a \rangle$, and depends only on C' . However, for larger values of C' there is an additional dependence on $\sigma_a / \langle a \rangle$, except at small $\sigma_a / \langle a \rangle$ (see the curves for $\sigma_a / \langle a \rangle = 0.0625$ and 0.125). The additional dependence on $\sigma_a / \langle a \rangle$ for large $\sigma_a / \langle a \rangle$ is because the assumption of small local aperture perturbations required in deriving (5) is violated.

For each of the aperture/entrapped-phase fields summarized in **Figure 2**, we simulated flow of the saturated wetting phase. **Figure 3** shows the entrapped phase structures in gray for $C' = 0.0, 2.14, \text{ and } 4.29$ in the $\sigma_a / \langle a \rangle = 0.0625$ aperture field. As C' increases, the flowing phase becomes more connected and less tortuous. **Figure 4** shows cumulative entrapped-area distributions for $C' = 0.27, 1.09, \text{ and } 2.14$ at each value of $\sigma_a / \langle a \rangle$. **Figure 4** incrementally sums a sorted list of the area occupied by each discrete entrapped region, beginning with the smallest regions. **Figure 4** demonstrates that approximately 20% of the largest non-wetting phase regions account for all but about 0.03 of the total area occupied by non-wetting phase. However, it is clear from the phase-

distribution fields in **Figure 3** that the smallest 80% of the entrapped regions will significantly influence flow of the wetting phase through the fracture. The cumulative-entrapped-area distributions plotted in **Figure 4** also allow a quantitative evaluation of the ability of C' to predict entrapped phase structures over a range of aperture-field statistics. For $C' = 0.27$ the cumulative-entrapped-area distributions are in close agreement for all values of $\sigma_a / \langle a \rangle$. Furthermore, for all values of C' , the plots for $\sigma_a / \langle a \rangle = 0.0625$ and 0.125 are in agreement over the entire range of entrapped-region sizes. However, for larger values of both C' and $\sigma_a / \langle a \rangle$, the cumulative-entrapped-area distributions begin to deviate. Again, these deviations result from the violation of the small perturbation assumption inherent in the definition of C' .

3.3 Flow simulations

The ratio of the simulated flow-rate through each saturated field to the simulated flow rate through the saturated field provides estimates of k_{rw} for each field. **Figure 5** shows k_{rw} plotted against S_f for all of the simulated entrapped-phase distributions. For each value of $\sigma_a / \langle a \rangle$, k_{rw} follows a similar functional relationship with S_f , regardless of $\sigma_a / \langle a \rangle$. The only significant scatter occurs at the smallest values of S_f , or for the entrapped-phase distributions corresponding to $C' = 0$. S_f measures only the fractional volume of the entrapped phase and provides no information about the entrapped-phase structure. However, C' is intrinsically linked to the entrapped-phase structure and thus may provide a better parameter for estimating k_{rw} . Plotting k_{rw} against C' (**Figure 6**) demonstrates that for small values of C' , C' provides a more reliable single parameter than S_f , for estimating k_{rw} . However, for larger values of C' (smaller S_f), particularly for $\sigma_a / \langle a \rangle = 0.5$, S_f is an effective single parameter for estimating k_{rw} .

We estimated τ using the approach of *Nicholl et al.* [2000]; by simulating flow through each phase geometry in the absence of aperture variability (i.e. $a=1$ for flowing phase, $a=0$ for the entrapped phase) (4) can be simplified to $k_{rw} = S_f \tau$. **Table 1** compares simulated estimates of k_{rw} to estimates based on (7), and presents each of the individual contributions to (7). As observed by *Nicholl et al.* [2000], τ has the most significant influence on the estimate of k_{rw} , with S_f having a secondary influence. As $\sigma_a / \langle a \rangle$ increases, the role of part A in (7) increases, especially for small C' , and changes in aperture variability (quantified by part B) have a negligible influence on predicted k_{rw} for all values of $\sigma_a / \langle a \rangle$ and C' . **Figure 7** plots simulated versus predicted k_{rw} and demonstrates that, across the ranges of $\sigma_a / \langle a \rangle$ and C' investigated here, (7) provides very good estimates of k_{rw} .

4.0 Summary

We have presented a preliminary investigation of the parameters that influence saturated relative permeability in variable-aperture fractures. Nondimensionalizing a first-order perturbation expansion of the Laplace-Young equation suggested that a dimensionless modified curvature number (C') will control the nature of the entrapped phase structure resulting from the slow invasion of an immiscible fluid into a horizontal fracture. Subsequent simulations of wetting-fluid invasions supported these results for $\sigma_a / \langle a \rangle$ less than about 0.25. For larger values of $\sigma_a / \langle a \rangle$, the assumption of small local aperture perturbations is no longer valid, and differences in the entrapped phase structure begin to occur.

Simulations of flow of the saturated wetting phase provided estimates of the saturated relative permeability for different values of C' and $\sigma_a / \langle a \rangle$. Our results support the use of the conceptual model presented by Nicholl et al. [2000] to describe k_{rw} over a wider range of parameters than they investigated. Additionally, the tortuosity factor is consistently the most significant contribution to k_{rw} . However, we have quantified τ by simulating flow through the entrapped-phase field in the absence of variability; this is computationally costly and thus, it would be useful to develop an independent measure of τ as a function of entrapped phase statistics.

Acknowledgments: Funding for this work was provided by the Department of Energy's Office of Basic Energy Sciences, Geosciences Program under contract numbers DE-FG03-96ER14590 (University of Colorado), DE-AC04-94AL85000 (Sandia National Laboratories), and DE-FG03-99ER14944 (University of Idaho). This work was performed under the auspices of the U. S. Department of Energy by the University of California, Lawrence Livermore National Laboratory under Contract No. W-7405-Eng-48.

References

- Brown, S. R., A simple mathematical model of a rough fracture, *J. Geophys. Res.*, 100(B4), 5941–5952, 1995.
- Glass, R.J., L. Yarrington, and M.J. Nicholl, A modified invasion percolation model for low capillary number immiscible displacements in horizontal rough walled fractures: Influence of local in-plane curvature, *Water Resour. Res.*, 34, 3215-34, 1998.
- Glass, R.J., L. Yarrington, and M.J. Nicholl, Correction to "A modified invasion percolation model for low capillary number immiscible displacements in horizontal rough walled fractures: Influence of local in-plane curvature", *Water Resour. Res.*, 36, 1991, 2000.
- Nicholl, M.J., H. Rajaram, and R.J. Glass, Factors controlling saturated relative permeability in a partially-saturated horizontal fracture, *Geophys. Res. Lett.*, 27, 393-396, 2000.
- Zimmerman, R.W. and G.S. Bodvarsson, Hydraulic conductivity of rock fractures, *Trans. Porous Media*, 23, 1-30, 1996.

Table 1: Simulated and predicted (based on (7)) k_{rw} and parameters used in evaluating (7).

| $\sigma_a / \langle a \rangle$ | C' | k_{rw} | | τ | S_f | part A | part B |
|--------------------------------|------|-----------|-----------|--------|-------|--------|--------|
| | | simulated | predicted | | | | |
| 0.0625 | 0.00 | 0.04 | 0.04 | 0.08 | 0.44 | 0.91 | 1.01 |
| | 0.27 | 0.08 | 0.08 | 0.17 | 0.47 | 0.92 | 1.01 |
| | 0.54 | 0.11 | 0.11 | 0.21 | 0.53 | 0.93 | 1.01 |
| | 1.07 | 0.17 | 0.17 | 0.29 | 0.61 | 0.96 | 1.00 |
| | 2.14 | 0.37 | 0.37 | 0.49 | 0.75 | 0.98 | 1.00 |
| | 4.29 | 0.82 | 0.82 | 0.87 | 0.95 | 1.00 | 1.00 |
| | 8.58 | 1.00 | 1.00 | 1.00 | 1.00 | 1.00 | 1.00 |
| 0.125 | 0.00 | 0.03 | 0.03 | 0.08 | 0.42 | 0.82 | 1.03 |
| | 0.27 | 0.07 | 0.07 | 0.18 | 0.45 | 0.84 | 1.03 |
| | 0.54 | 0.11 | 0.11 | 0.22 | 0.52 | 0.87 | 1.02 |
| | 1.07 | 0.16 | 0.16 | 0.28 | 0.58 | 0.91 | 1.02 |
| | 2.14 | 0.40 | 0.39 | 0.53 | 0.75 | 0.96 | 1.01 |
| | 4.29 | 0.93 | 0.93 | 0.95 | 0.98 | 1.00 | 1.00 |
| | 8.58 | 1.00 | 1.00 | 1.00 | 1.00 | 1.00 | 1.00 |
| 0.25 | 0.00 | 0.03 | 0.03 | 0.08 | 0.38 | 0.65 | 1.07 |
| | 0.27 | 0.06 | 0.06 | 0.17 | 0.41 | 0.71 | 1.06 |
| | 0.54 | 0.10 | 0.10 | 0.23 | 0.49 | 0.76 | 1.05 |
| | 1.07 | 0.19 | 0.19 | 0.33 | 0.60 | 0.84 | 1.03 |
| | 2.14 | 0.44 | 0.45 | 0.56 | 0.81 | 0.95 | 1.01 |
| | 4.29 | 0.99 | 0.99 | 0.99 | 0.99 | 1.00 | 1.00 |
| | 8.58 | 1.00 | 1.00 | 1.00 | 1.00 | 1.00 | 1.00 |
| 0.5 | 0.00 | 0.02 | 0.02 | 0.08 | 0.29 | 0.39 | 1.00 |
| | 0.27 | 0.03 | 0.03 | 0.14 | 0.30 | 0.43 | 1.00 |
| | 0.54 | 0.05 | 0.04 | 0.19 | 0.34 | 0.48 | 1.00 |
| | 1.07 | 0.09 | 0.08 | 0.25 | 0.44 | 0.59 | 1.00 |
| | 2.14 | 0.23 | 0.23 | 0.41 | 0.63 | 0.78 | 0.99 |
| | 4.29 | 0.71 | 0.71 | 0.83 | 0.88 | 0.95 | 1.00 |
| | 8.58 | 0.99 | 0.99 | 1.00 | 1.00 | 1.00 | 1.00 |

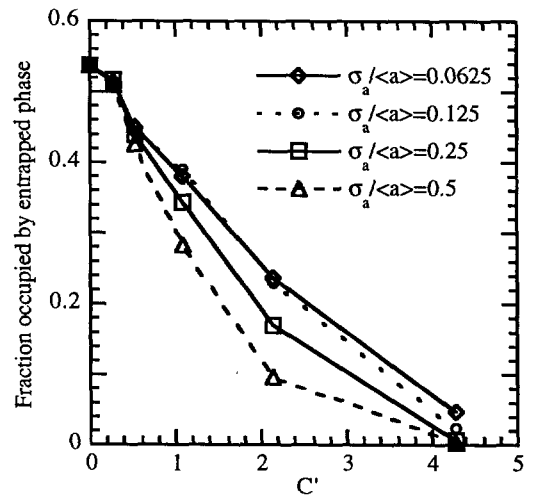
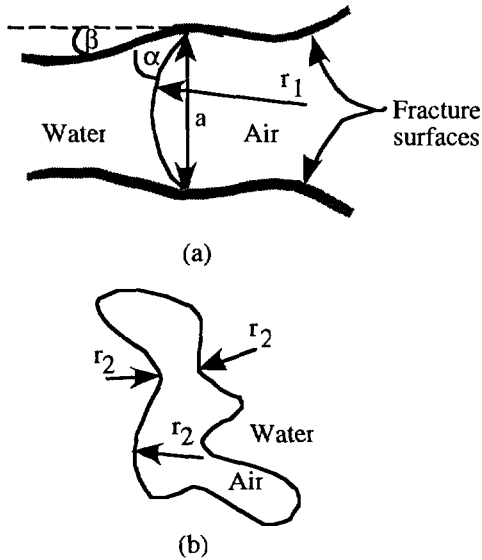
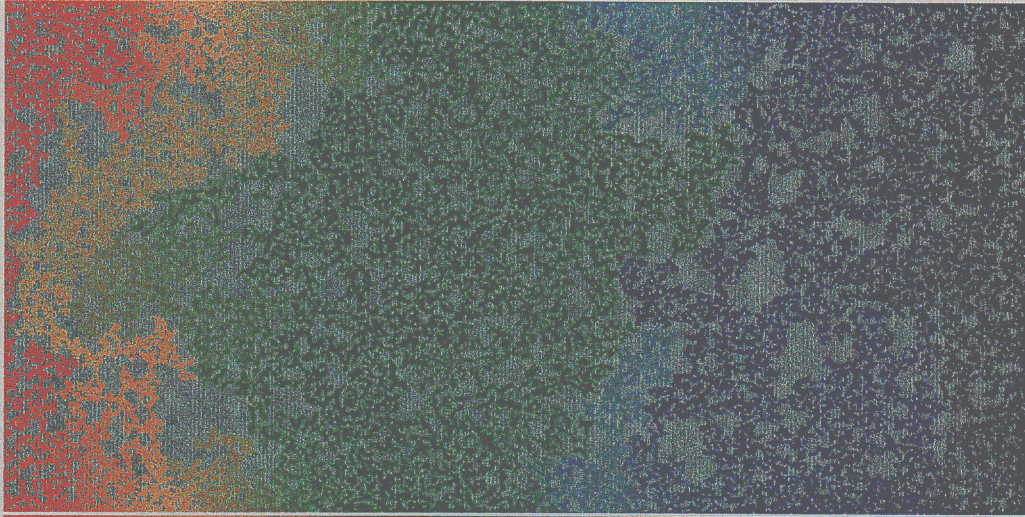


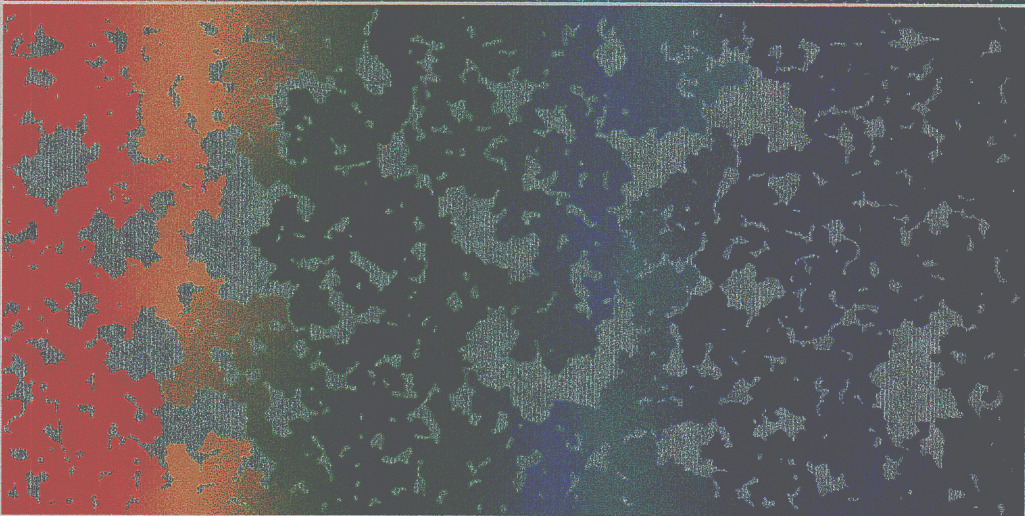
Figure 2: S versus C' .

Figure 1: Schematic cross section (a) and plan view (b) of an air water interface exhibiting both out-of-plane (r_1) and in-plane (r_2) curvature.

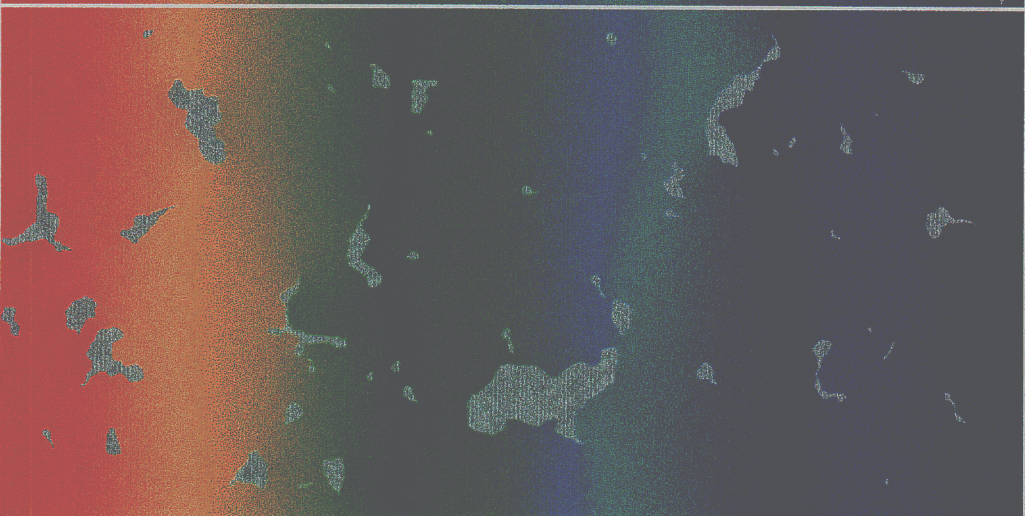
$C = 0.0$



$C = 2.14$



$C = 4.29$



$h/h_c = 1$



$h/h_c = 0$

Figure 3: Pressure fields from flow simulations in the $\sigma_a / \langle a \rangle = 0.0625$ aperture / entrapped-phase fields resulting from a uniform pressure head applied to the left ($h=h_0$) and right ($h=0$) edges of the domain. Gray represents the entrapped non-wetting phase.

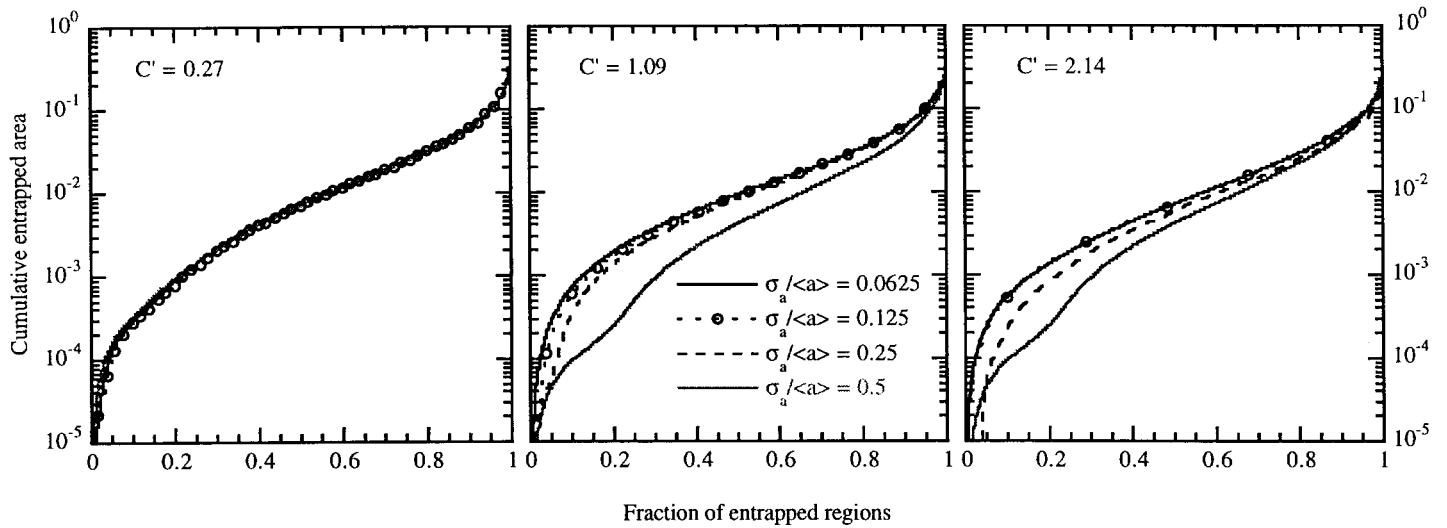


Figure 4: Cumulative entrapped area (S_e) versus fraction of the entrapped regions.

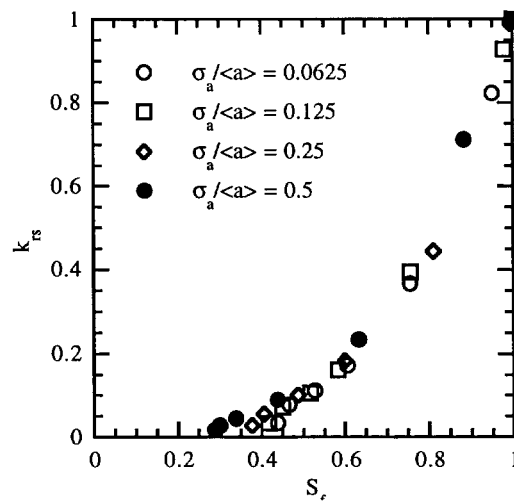


Figure 5: k_{rw} versus S_f .

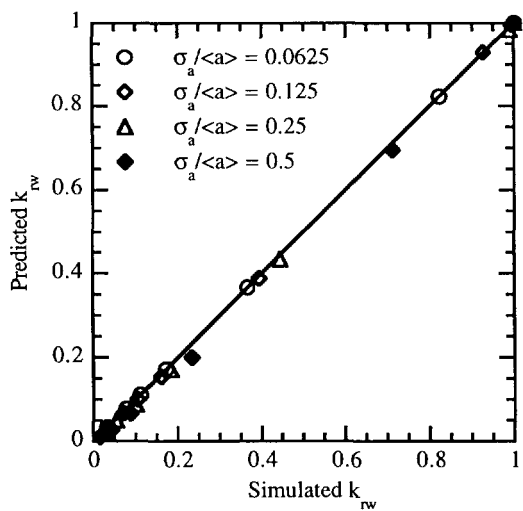


Figure 6: Predicted vs. simulated k_{rw} .

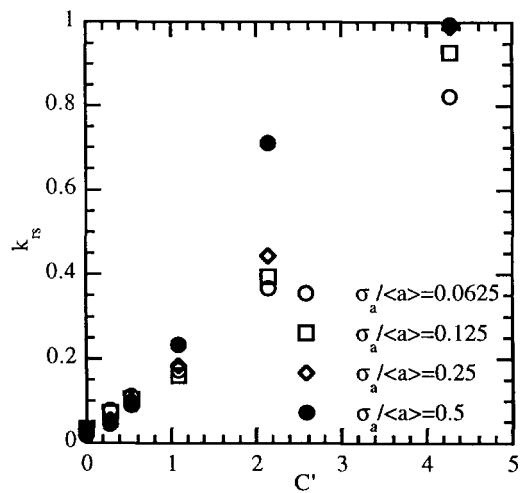


Figure 7: k_{rw} vs. C'